NEOPLASMA accepted, ahead of print manuscript
Cite article as https://doi.org/10.4149/neo_2026_250923N408

Running title: Apatinib and cinobufagin in gastric cancer

Targeting the MDM2/Caspase-3/GSDME axis: apatinib and cinobufagin synergistically induce pyroptosis to suppress gastric cancer progression

Lei Cao[1,#], Lijuan Meng[2,#], Yueyao Lu[2], Lixin Yang[2], Weiyou Zhu[2,*]

[1]Department of Oncology, The Affiliated Suqian First People's Hospital of Nanjing Medical University, Suqian, Jiangsu, China; [2]Department of Oncology, The First Affiliated Hospital of Nanjing Medical University, Nanjing, Jiangsu, China

*Correspondence: zhuweiyou_Zwy@163.com

[#]Contributed equally to this work.

Received September 23, 2025 / Accepted July 3, 2026

Gastric cancer (GC) is a highly heterogeneous and aggressive malignancy with a poor prognosis, especially in advanced stages. Apatinib and cinobufagin (CS-1) have shown promising antitumor potential. However, the therapeutic efficacy and underlying mechanisms of their combined use in GC remain unclear. GC cell lines (AGS and GPM-1) were treated with apatinib, CS-1, or both. Cell viability, proliferation, migration, apoptosis, stemness, and pyroptosis-related protein expression were evaluated using cell counting kit-8 (CCK-8), colony formation, wound healing assays, flow cytometry, tumorsphere assays, and western blotting. The role of mouse double minute 2 homolog (MDM2) in modulating treatment response was investigated via overexpression experiments. Antitumor efficacy in vivo was assessed using a subcutaneous xenograft mouse model, and tumor apoptosis and proliferation were analyzed by terminal deoxynucleotidyl transferase dUTP nick end labeling (TUNEL) and immunohistochemistry. Combined treatment with apatinib and CS-1 significantly inhibited GC cell viability, proliferation, migration, and stemness, while inducing apoptosis and pyroptosis more effectively than either agent alone. Mechanistically, the combination therapy downregulated MDM2 expression and upregulated cleaved caspase-3 (C-caspase-3) and gasdermin E-N (GSDME-N). Overexpression of MDM2 partially reversed these effects both in vitro and in vivo, leading to reduced apoptosis, pyroptosis, and antitumor efficacy. Apatinib combined with CS-1 synergistically suppresses GC progression by inducing MDM2/C-caspase-3/GSDME-regulated pyroptosis. These findings highlight MDM2 as a critical therapeutic target and provide novel insights into the molecular mechanisms underlying the combined use of targeted agents and natural compounds in GC therapy.

Key words: gastric cancer; apatinib; cinobufagin; mouse double minute 2 homolog; pyroptosis

Gastric cancer (GC), a common and aggressive malignancy originating from the gastric mucosal

epithelium, exhibits marked heterogeneity and invasiveness [1, 2]. According to global cancer epidemiological data, GC ranks fifth in incidence and fourth in cancer-related mortality worldwide, approximately 1.089 million new cases and 769,000 deaths in 2020. GC is highly prevalent in East Asia and shows an increasing incidence among young patients, posing a serious threat to public health [3]. Current therapeutic approaches for GC include surgical resection, radiotherapy, chemotherapy, molecular targeted therapy, and, more recently, immunotherapy [4, 5]. Despite advancements in multimodal treatment strategies, the prognosis for patients with advanced GC remains poor, with low five-year survival rates and high risks of recurrence and metastasis [6]. This is largely due to the insidious nature of early GC symptoms, leading to diagnosis at advanced stages, and the lack of reliable early diagnostic markers and effective therapeutic targets. Therefore, elucidating the molecular mechanisms underlying GC development, identifying specific diagnostic and prognostic biomarkers, and developing more effective treatment strategies are crucial to improving clinical outcomes.

Cinobufagin (CS-1), a bioactive bufadienolide compound extracted from the traditional Chinese medicine Bufo bufonis, has demonstrated notable antitumor and anti-inflammatory activities [7]. CS-1 has shown promising therapeutic effects in various tumor models. Previous studies have reported that CS-1 inhibits tumor progression in non-small cell lung cancer by blocking the signal transducer and activator of transcription 3 (STAT3) signaling pathway [8]. Additionally, CS-1 suppresses ovarian cancer progression by regulating vasculogenic mimicry and modulating the activity of tumor-associated macrophages [9]. It also inhibits hepatocellular carcinoma growth by upregulating cuproptosis-related genes [10]. It is noteworthy that a recent proteomic study has revealed that CS-1 exerts anti-gastric cancer effects through inhibiting proliferation and inducing apoptosis [11]. Apatinib, a small-molecule tyrosine kinase inhibitor, competitively binds to the intracellular ATP-binding site of VEGFR-2 to block downstream signal transduction. Beyond inhibiting angiogenesis, it can also directly induce multiple forms of programmed cell death in tumor cells, including apoptosis, autophagy, and ferroptosis [12, 13]. Apatinib induces apoptosis, autophagy, and ferroptosis depending on the cell context, while CS-1 induces apoptosis and cuproptosis, at least. Thus, it is useful to investigate the mechanism of cell death of the combination of apatinib and CS-1. In this study, we investigated the inhibitory effects of apatinib combined with CS-1 on GC cells, with a particular focus on elucidating the underlying mechanism of cell death induced by this combination.

Given that apatinib and CS-1 induce distinct forms of programmed cell death depending on cellular context, we sought to systematically characterize the cell death modality and molecular pathways involved in their synergistic anti-tumor activity. Our findings aim to provide mechanistic insights and experimental support for the clinical translation of this combination therapy in GC treatment.

Materials and Methods

Animal ethics. Vitalriver (China) supplied twenty-four female immunodeficient BALB/c nude mice (5 weeks old, 15-20 g). All animal experiments were authorized by Zhejiang Baiyue Biotechnology Co., Ltd.'s Ethics Committee (Approval No. ZJBYLA-IACUC-20241205) and carried out in accordance with the rules for the care and use of laboratory animals. Mice were kept in controlled environments with a 12-hour light/dark cycle, a temperature of 22±2 °C, and a humidity of 55±10%. They also had unrestricted access to water and normal laboratory chow. To reduce physiological alterations brought on by stress, animals were acclimated to lab conditions for a minimum of one week before to tests.

Cell Culture. Dulbecco's Modified Eagle Medium (DMEM; #C0891, Beyotime, China) was applied to cultivate the human GC cell lines AGS (#AW-CH0029, AnWei-sci, China) and GPM-1 (#NTCC-S833, BioVector NTCC Inc., China). It was also supplemented with 10% fetal bovine serum (FBS; #10100139, ThermoFisher, USA) and 1% penicillin-streptomycin (#C0222, Beyotime, China). The cells were kept at 37 °C with 5% CO_2 in a humidified incubator (#D165H, Rwdls, China). Cell line identification was verified by short tandem repeat profiling.

Cell treatment. The MDM2 overexpression vector (pRP[Exp]-CMV>hMDM2 [NM_002392.6]) and negative control (oe-NC) were purchased from VectorBuilder (China). Six sets of AGS and GPM-1 cells were created: control (Con), Apatinib, CS-1, Apatinib+CS-1, Apatinib+CS-1+oe-NC, and Apatinib+CS-1+oe-MDM2. For 24 h, cells in the Apatinib group were exposed to 5 μM apatinib (#S2221, Selleck, China) [14]. For 24 h, 0.05 μM CS-1 (#S3224, Selleck, China) was administered to the CS-1 group [15]. For 24 h, the Apatinib+CS-1 group was treated with 5 μM apatinib and 0.05 μM CS-1. Lipofectamine 2000 (#11668019, Invitrogen, USA) served to transfect cells with the corresponding vectors for the Apatinib+CS-1+oe-NC and Apatinib+CS-1+oe-MDM2 groups. Reverse transcription quantitative polymerase chain reaction (RT-qPCR) was utilized to assess transfection efficiency 48 h after transfection. After that, cells were exposed to 0.05 μM CS-1 and 5

μM apatinib for a full day.

Cell counting kit-8 (CCK-8) assay. The CCK-8 test kit (#C0038, Beyotime, China) was employed to evaluate cell viability in accordance with the manufacturer's instructions. In short, 96-well plates (#FCP962, Beyotime, China) were planted with GC cells. Following the specified treatments, 10 μl of CCK-8 solution was added to each well, and the wells were then incubated for 2 h. A microplate reader (Bio-Rad, CA, USA) was deployed to detect absorbance (450 nm).

Drug combination synergy assay. To evaluate the synergistic interaction between apatinib and CS-1, gastric cancer cells (GPM-1 and AGS) were seeded in 96-well plates at a density of 5×10^3 cells/well and incubated overnight. Cells were then treated with apatinib and CS-1, either alone or in combination at a fixed molar ratio of 100:1 (based on the IC50 ratio of the two drugs in each cell line), for 48 h. Cell viability was measured using the CCK-8 assay as described above. The Chou-Talalay method based on the median-effect principle was adopted, and CompuSyn software (ComboSyn Inc., USA) was used to calculate the combination index (CI). $CI < 1$ indicates synergism, $CI=1$ indicates additivity, and $CI > 1$ indicates antagonism.

Colony formation assay. 6-well plates (#FCP060, Beyotime, China) were seeded with GC cells (five thousand cells per well). Following an overnight incubation period, cells were exposed to the corresponding treatments before being cultivated for two weeks in fresh media. For 5 min, colonies were stained with 0.1% crystal violet (#C0121, Beyotime, Shanghai, China) after being fixed with 4% paraformaldehyde (#P0099, Beyotime, China). A camera (Nikon, Japan) was implemented to take pictures of the colonies, and the total number of colonies was tallied. The colony formation rate was calculated as: (number of colonies/number of cells seeded) × 100% [16].

Wound healing assay. Following treatments, GC cells were cultivated to nearly 100% confluence in 6-well plates. A sterile 10 μl pipette tip (#PTB00122, Vazyme, China) was utilized to make a scratch on the cell monolayer in each well. To evaluate the ability of cells to migrate, wound closure was monitored and photographed at 0 h and 24 h using an optical microscope (×100, Nikon Eclipse 80i, Japan).

Flow cytometry. Annexin V-fluorescein isothiocyanate (FITC) and propidium iodide (PI) double staining (#640914, BioLegend, USA) was utilized to identify GC cell apoptosis. Cells were collected 48 hours after the respective treatments, centrifuged, and then resuspended in 200 μl of binding buffer. After adding 10 μl of Annexin V-FITC and 5 μl of PI, the mixture was incubated for 15 min in the

dark. 300 µl of binding buffer was then added. Using a FACSCalibur device (BD Biosciences, USA), flow cytometry was executed to gauge apoptosis.

Sphere formation assay. Serum-free DMEM/F12 medium (#11320033, ThermoFisher, USA) was applied to resuspend single-cell suspensions of treated GC cells supplemented with 100 µg/ml penicillin-streptomycin, 20 ng/ml human recombinant epidermal growth factor (EGF; #92708ES60, YEASEN, China), 10 ng/ml human recombinant basic fibroblast growth factor (bFGF; #91330ES10, YEASEN, China), 2% B27 supplement without vitamin A (#12587010, ThermoFisher, USA), and 1% N2 supplement (#C0335, Beyotime, China). Ultra-low attachment 6-well plates (#3471, Corning, USA) were applied for cell seeding. Following a 6-day culture period, the total number of tumor spheres was counted using optical microscope (×200).

RT-qPCR. Following the manufacturer's instructions, TRIzol reagent (#A33250, ThermoFisher, USA) was applied to extract total RNA from GC cells. Reverse transcription was performed to create complementary DNA (cDNA) (#04379012001, Roche, USA). SYBR Green PCR Master Mix (#4344463, ThermoFisher, USA) was implemented in quantitative real-time PCR on an ABI PRISM 7300 RT-PCR system (Applied Biosystems, USA). The internal control was glyceraldehyde-3-phosphate dehydrogenase (GAPDH). The $2^{-\Delta\Delta CT}$ technique was used to determine relative gene expression levels [17]. Table 1 lists primer sequences created by Tsingke (Beijing, China).

Western blot analysis. GC cells and tumor tissues were treated with radioimmunoprecipitation assay (RIPA) buffer (#P0013, Beyotime, China) to extract proteins. The bicinchoninic acid assay kit (#P0009, Beyotime, Shanghai, China) served to measure the quantities of proteins. Using sodium dodecyl sulfate-polyacrylamide gel electrophoresis (#P0690, Beyotime, Shanghai, China), protein samples (30 µg) were separated and then put onto polyvinylidene fluoride membranes (#FFP24, Beyotime, China). Membranes were blocked for 2 h with 5% non-fat milk, then incubated with primary antibodies for the entire night and then with secondary antibodies for an additional 60 min. Table 2 offers comprehensive details about antibodies. An improved chemiluminescence detection kit (#KGC4902, Keygene, China) and gel imaging equipment (Bio-Rad, USA) were utilized to visualize protein bands. Loading control was implemented using GAPDH. ImageJ software (NIH, USA) was adopted to quantify band intensities.

Animal treatment. Either the MDM2 overexpression plasmid or the negative control (oe-NC)

plasmid was employed to transfect GPM-1 cells. Cells were again suspended in phosphate-buffered saline (PBS; #ST341, Beyotime, China) after 48 h. To create a subcutaneous tumor model, each mouse received a subcutaneous injection of 200 μl of cell suspension (2.5×10^4 cells/μl) [18]. Animals were randomly divided into three groups (n=8/group): Con+oe-NC, Apatinib+CS-1+oe-NC, and Apatinib+CS-1+oe-MDM2. GPM-1 cells transfected with the NC plasmid served to inoculate the Con+oe-NC and Apatinib+CS-1+oe-NC groups, whereas GPM-1 cells transfected with the MDM2 plasmid were given to the Apatinib+CS-1+oe-MDM2 group. Mice in the Apatinib+CS-1+oe-NC and Apatinib+CS-1+oe-MDM2 groups received intravenous injections of Apatinib (7.5 mg/kg) and CS-1 (0.2 mg/kg) via tail vein every two days once the tumor volume had grown to about 100 mm^3 [19]. Equal amounts of physiological saline (#ST341, Beyotime, China) were given to the Con+oe-NC group. Day 1 was designated as the first injection day. Every two days, tumor volumes were measured. Mice were given sodium pentobarbital (80 mg/kg, #P3761, Sigma-Aldrich, USA) to induce anesthesia on day 17, and they were then put to death by cervical dislocation. Tumor tissues were gathered, and some were preserved in 4% paraformaldehyde and some were frozen for storage.

Terminal deoxynucleotidyl transferase dUTP Nick-End Labeling (TUNEL) assay. The tumor tissues were cut into 5 μm slices after being fixed in paraffin (#8002-74-2, Yuanyang, China). Sections were hydrated after being deparaffinized with xylene (#A530011-0500, Sangon, China). Sections were cleaned with phosphate-buffered saline (PBS; #0221A, Shanghai, China) following a 10 min treatment with 0.1% Triton X-100 (#ST797, Beyotime, China). After that, sections were incubated for an 1 h with 50 μl of TUNEL reaction mixture (#C1086, Beyotime, China). Following washing, 2-(4-amino-phenyl)-6-indolecarbamidine dihydrochloride (DAPI; #C1002, Beyotime, China) was employed to stain the nuclei for 10 min. An inverted fluorescence microscope (×400, Nikon, Japan) was set up to view the fluorescence signals. TUNEL-positive apoptotic cells fluoresced green, whereas DAPI-positive nuclei were blue.

Immunohistochemistry. Tumor tissues fixed in paraffin were cut into sections 5 μm thick. Following antigen retrieval with citrate buffer (#C2488, Sigma-Aldrich, USA), sections were blocked for 1 h with 5% bovine serum albumin (BSA; #ST025, Beyotime, China). Sections containing the primary antibody against Ki67 (#ab15580, Abcam, UK) were incubated for the entire night. Goat anti-rabbit IgG H&L (HRP) secondary antibody (#ab6721, Abcam, UK) was added to sections and

incubated for 1 hour following PBS washing. Hematoxylin (#H9627, Sigma-Aldrich, USA) was used as a counterstain after sections were cleaned and developed using the 3,3'-diaminobenzidine (DAB) substrate kit (#ab64238, Abcam, UK). Staining was seen using an optical microscope (400×). Staining that was positive looked brown.

Statistical analysis. The mean±standard deviation (SD) serves to display the data. Figure 6A was analyzed using two-way analysis of variance (ANOVA), whilst other group comparisons were analyzed utilising one-way ANOVA. Software called GraphPad Prism 8.0 (GraphPad, USA) was adopted to conduct statistical analyses. P-values below 0.05 were regarded as statistically significant.

Results

Apatinib combined with cinobufagin synergistically inhibits GC cell viability and induces apoptosis. To determine the optimal concentrations of Apatinib and CS-1, we examined the effects of different concentrations of Apatinib (1, 2.5, 5, 10 and 20 μM) and CS-1 (0.01, 0.025, 0.05, 0.1 and 0.2 μM) on the viability of GC cells. The result showed that both Apatinib and CS-1 at various concentrations significantly inhibited the viability of gastric cancer cells ($p < 0.05$, Figures 1A-1D). To evaluate whether apatinib and CS-1 exert synergistic effects, we performed combination experiments in GPM-1 and AGS cells using the Chou-Talalay method. The IC50 values were 9.813 μM (apatinib) and 0.1034 μM (CS-1) in GPM-1 cells, and 19.93 μM (apatinib) and 0.1267 μM (CS-1) in AGS cells. Based on these ratios, a fixed molar ratio of 100:1 (apatinib:CS-1) was used for combination experiments. The combination produced dose-dependent inhibition of cell viability, with effects markedly greater than either drug alone(Figures 1E-1H). Quantitative analysis revealed CI values consistently below 1 in both cell lines, indicating synergism (Table 3). These results demonstrate that apatinib and CS-1 exert synergistic inhibitory effects on gastric cancer cells.

When the concentration of Apatinib is greater than or equal to 5 μM and the concentration of CS-1 is greater than or equal to 0.05 μM, the inhibition of cell viability becomes the most significant. Therefore, these two concentrations were selected for the subsequent experiments. Treatment with apatinib and CS-1 lowered the viability, proliferation ($p < 0.05$, Figures 1I-1M), and migratory capacity of AGS and GPM-1 cells ($p < 0.05$, Figures 2A-2C). Compared to either medication alone, the combined treatment showed a larger inhibitory effect ($p < 0.01$, Figures 1I-1M, Figures 2A-2C). Furthermore, apatinib and CS-1 greatly boosted apoptosis and diminished stemness in GC cells,

with the combination outperforming single-agent treatments ($p < 0.05$, Figures 2D-2I). In both AGS and GPM-1 cells, apatinib and CS-1 therapy raised gasdermin E-N (GSDME-N) and cleaved caspase-3 (C-caspase-3) while suppressing MDM2 expression ($p < 0.05$, Figures 3A-3J). And the combined therapy has more noticeable regulatory effects ($p < 0.01$, Figures 3A-3J).

MDM2 overexpression attenuates the inhibitory effects of apatinib combined with CS-1 on GC cells. To explore these mechanisms, we utilized the SwissTargetPrediction database and identified multiple potential shared targets of apatinib and CS-1, and obtained 16 overlapping targets, including RET, PTGS2, PDGFRB, MTNR1B, MTNR1A, MDM2, KIT, KDR, IDH1, FNTAFNT, FGFR1, EGFR, CSF1R, CCNB3CD, CA1, and ABL1. Through literature-based screening for genes associated with pyroptosis, MDM2 was identified as the key target for further investigation [20, 21]. A plasmid that overexpresses MDM2 was created in order to investigate how MDM2 regulates GC cells in response to apatinib and CS-1. Transfection dramatically raised AGS and GPM-1 cells' MDM2 levels ($p < 0.001$, Figures 4A, 4B). The Apatinib+CS-1 group exhibited substantially lower cell viability, proliferation, and migration as compared to the Con group ($p < 0.01$, Figures 4C-4J). However, MDM2 overexpression partially reversed the inhibitory effects of Apatinib and CS-1 ($p < 0.05$, Figures 4C-4J). Similarly, apoptosis, GSDME-N and C-caspase-3 increased, and stemness diminished dramatically in the Apatinib+CS-1 group compared to Con group, while MDM2 overexpression notably weakened these effects ($p < 0.001$, Figures 5A-5K).

MDM2 overexpression weakens the antitumor effects of apatinib combined with CS-1 *in vivo*. After 13 days of treatment, the Apatinib+CS-1+oe-NC group's tumor volumes were noticeably smaller than those of the Con+oe-NC group ($p < 0.05$, Figures 6A, 6B); tumor volumes in the Apatinib+CS-1+oe-MDM2 group were noticeably greater than those in the Apatinib+CS-1+oe-NC group ($p < 0.01$, Figures 6A, 6B). Analysis revealed that tumors from the Apatinib+CS-1+oe-NC group had lower Ki67 expression (brown) and higher apoptosis (green) than those from the Con+oe-NC group (Figures 6C, 6D). On the other hand, compared to the Apatinib+CS-1+oe-NC group, tumors from the Apatinib+CS-1+oe-MDM2 group showed higher Ki67 levels and less apoptosis (Figures 6C, 6D). Furthermore, compared to Con+oe-NC, the Apatinib+CS-1+oe-NC group had considerably greater levels of GSDME-N and C-caspase-3, but MDM2 overexpression resulted in a large drop in these protein levels. ($p < 0.05$, Figures 6E-6G).

Discussion

This study demonstrates that the combination of apatinib and CS-1 significantly suppresses the proliferation, migration, and stemness of GC cells. The combined treatment not only inhibits tumor growth *in vitro* but also exerts potent antitumor effects *in vivo*, as evidenced by reduced tumor volumes and increased apoptosis in tumor-bearing mice. Further mechanistic investigation revealed that this synergistic antitumor activity is associated with the marked downregulation of MDM2 expression in GC cells. MDM2 is a critical E3 ubiquitin ligase that plays key roles in regulating the cell cycle, apoptosis, and tumorigenesis [22]. In retinoblastoma, MDM2 promotes cancer cell survival by modulating the expression of hypoxia-inducible factor 1-alpha (HIF-1α) and von hippel-lindau protein (pVHL) [23]. In colorectal cancer, MDM2 contributes to chemotherapy resistance by degrading inhibitor of growth family member 3 (ING3) [24]. Additionally, in ovarian cancer, human males absent on the first (hMOF) promotes cisplatin resistance through stabilization of MDM2 [25]. MDM2 has also been reported to act as an oncogene in GC [26]. Previous studies suggest that both apatinib and CS-1 can suppress MDM2 expression [15, 27]. Our findings further demonstrate that MDM2 overexpression partially reverses the antitumor effects of apatinib combined with CS-1, indicating that MDM2 suppression may underlie the therapeutic synergy.

Pyroptosis is a form of programmed cell death characterized by pore formation in the plasma membrane, leading to cell swelling, membrane rupture, and the release of pro-inflammatory cytokines [28, 29]. Unlike classical apoptosis, pyroptosis plays a unique and pivotal role in modulating the tumor immune microenvironment and antitumor immunity [30, 31]. Recent studies have highlighted the involvement of pyroptosis in tumor progression, metastasis, and drug resistance. For example, Tanshinone I induces pyroptosis in cisplatin-resistant GC cells via the nuclear factor kappa-light-chain-enhancer of activated B cells (NF-κB)/caspase-3/8/gasdermin E (GSDME) pathway [32]. Centromere protein M (CENPM) knockdown activates the cyclic GMP-AMP synthase (cGAS)-stimulator of interferon genes (STING) pathway, thereby enhancing pyroptosis and suppressing ovarian cancer progression [33]. Conversely, chemotherapy-induced pyroptosis mediated by GSDME has been linked to increased progression and resistance in pancreatic cancer [34]. At the molecular level, caspase-3, a key executioner of apoptosis, can also cleave GSDME to release its N-terminal domain, which forms pores in the cell membrane and triggers pyroptosis [35]. Thus, the caspase-3/GSDME axis constitutes a central execution pathway

of pyroptosis. In line with this, our results show that apatinib combined with CS-1 increases the expression of C-caspase-3 and GSDME-N in GC cells, initiating early-stage pyroptotic activity. Importantly, MDM2 overexpression reverses these effects, suggesting that MDM2 negatively regulates pyroptosis by inhibiting the C-caspase-3/GSDME pathway. Unlike the canonical MDM2- p53- dependent mitochondrial apoptotic pathway, the cell death mode triggered by apatinib plus CS- 1 is dominated by pyroptosis rather than classical apoptosis. Such a phenotypic switch may be attributed to the robust cellular stress induced by the combined treatment, which redirects activated caspase-3 to cleave GSDME rather than target apoptotic substrates. These findings highlight a non- apoptotic function of MDM2 in regulating pyroptosis, expanding our understanding of MDM2- mediated cell death programs in gastric cancer. It is noteworthy that the functional consequence of MDM2 modulation appears to be context-dependent. While MDM2 inhibitors such as Nutlin-3 are known to induce apoptosis through p53 stabilization in certain cancer types [36], our findings demonstrate that MDM2 downregulation by apatinib plus CS-1 promotes pyroptosis via the caspase-3/GSDME pathway in gastric cancer cells. This phenotypic divergence may be attributed to differences in p53 status, the intensity of cellular stress, and the substrate preference of activated caspase-3 under distinct therapeutic conditions. Collectively, these findings indicate that apatinib and CS-1 may suppress GC progression by downregulating MDM2 and activating pyroptosis, providing a novel therapeutic strategy targeting MDM2-mediated cell death.

Despite these encouraging results, this study has several limitations. First, the *in vivo* experiments were conducted using a subcutaneous tumor model, which may not fully replicate the complex tumor microenvironment of GC in patients. Future validation using clinical samples and patient-derived models is needed to confirm the translational relevance of these findings. Second, although this study focused on the MDM2/caspase-3/GSDME-mediated pyroptosis pathway, the precise upstream regulatory mechanisms remain to be elucidated.

In summary, this study confirms that the combination of apatinib and CS-1 synergistically inhibits GC cell viability, proliferation, migration, and stemness. The combined treatment induces pyroptosis by downregulating MDM2, thereby relieving its negative regulation on the C-caspase-3/GSDME pyroptosis execution pathway. Notably, MDM2 overexpression weakens the antitumor effects of apatinib and CS-1 both *in vitro* and *in vivo*, indicating that MDM2 is a key regulatory node. These findings provide new insights into the molecular mechanisms underlying the

synergistic effect of apatinib and CS-1 in GC therapy. This study lays a theoretical foundation for further clinical evaluation of this combination strategy and offers new potential for improving outcomes in patients with advanced GC.

Acknowledgements: This study was supported by the institutional budget.

References

[1] PARK YS, KOOK MC, KIM BH, LEE HS, KANG DW et al. A Standardized Pathology Report for Gastric Cancer: 2nd Edition. J Gastric Cancer 2023; 23: 107-145. https://doi.org/10.5230/jgc.2023.23.e7

[2] CHRISTODOULIDIS G, KOUMARELAS KE, KOULIOU MN, THODOU E, SAMARA M. Gastric Cancer in the Era of Epigenetics. International journal of molecular sciences 2024; 25: 3381. https://doi.org/10.3390/ijms25063381

[3] KANG K, BAGAOISAN MA, ZHANG Y. Unveiling the Younger Face of Gastric Cancer: A Comprehensive Review of Epidemiology, Risk Factors, and Prevention Strategies. Cureus 2024; 16: e62826. https://doi.org/10.7759/cureus.62826

[4] GUAN WL, HE Y, XU RH. Gastric cancer treatment: recent progress and future perspectives. J Hematol Oncol 2023; 16: 57. http://doi.org/10.1186/s13045-023-01451-3

[5] SONG Z, WU Y, YANG J, YANG D, FANG X. Progress in the treatment of advanced gastric cancer. Tumour Biol 2017; 39: 1010428317714626. https://doi.org/10.1177/1010428317714626

[6] JIN X, LIU Z, YANG D, YIN K, CHANG X. Recent Progress and Future Perspectives of Immunotherapy in Advanced Gastric Cancer. Front Immunol 2022; 13: 948647. https://doi.org/10.3389/fimmu.2022.948647

[7] DAI CL, ZHANG RJ, AN P, DENG YQ, RAHMAN K et al. Cinobufagin: a promising therapeutic agent for cancer. J Pharm Pharmacol 2023; 75: 1141-1153. https://doi.org/10.1093/jpp/rgad059

[8] YAN S, MA C, ZHOU F, ZHENG H, YANG L et al. Cinobufagin exerts an antitumor effect in non-small-cell lung cancer by blocking STAT3 signaling. J Cancer 2023; 14: 3309-3320. https://doi.org/10.7150/jca.86544

[9] WANG N, YANG Y, WANG H, LI Y, WANG M et al. Cinobufagin modulates vasculogenic mimicry and tumor-associated macrophages to inhibit ovarian cancer progression. Eur J Pharmacol 2025; 987: 177157. https://doi.org/10.1016/j.ejphar.2024.177157

[10] AMELIMOJARAD M, AMELIMOJARAD M, SHARIATI P. Cinobufagin treatments suppress tumor growth by enhancing the expression of cuproptosis-related genes in liver cancer. Naunyn Schmiedebergs Arch Pharmacol 2025; 398: 1575-1582. https://doi.org/10.1007/s00210-024-03349-4

[11] WANG P, ZHANG X, MA H, ZHANG Y. Exploring the mechanism of cinobufagin on gastric cancer based on proteomics, molecular dynamics, in vitro and in vivo experiment. Toxicol Appl Pharmacol 2025; 503: 117490. https://doi.org/10.1016/j.taap.2025.117490

[12] LI J, ZHAO X, CHEN L, GUO H, LV F et al. Safety and pharmacokinetics of novel selective vascular endothelial growth factor receptor-2 inhibitor YN968D1 in patients with advanced malignancies. BMC Cancer 2010; 10: 529. https://doi.org/10.1186/1471-2407-10-529

[13] XIE C, ZHOU X, LIANG C, LI X, GE M et al. Apatinib triggers autophagic and apoptotic cell death via VEGFR2/STAT3/PD-L1 and ROS/Nrf2/p62 signaling in lung cancer. J Exp Clin Cancer Res 2021; 40: 266. https://doi.org/10.1186/s13046-021-02069-4

[14] KE W, ZHANG L, ZHAO X, LU Z. p53 m(6)A modulation sensitizes hepatocellular carcinoma to apatinib through apoptosis. Apoptosis 2022; 27: 426-440. https://doi.org/10.1007/s10495-022-01728-x

[15] DENG X, SHENG J, LIU H, WANG N, DAI C et al. Cinobufagin Promotes Cell Cycle Arrest and Apoptosis to Block Human Esophageal Squamous Cell Carcinoma Cells Growth via the p73 Signalling Pathway. Biol Pharm Bull 2019; 42: 1500-1509. https://doi.org/10.1248/bpb.b19-00174

[16] BEMIDINEZHAD A, MIRZAVI F, GHOLAMHOSSEINIAN H, GHEYBI F, SOUKHTANLOO M. Gold-containing liposomes and glucose-coated gold nanoparticles enhances the radiosensitivity of B16F0 melanoma cells via increasing apoptosis and ROS production. Life Sci 2023; 318: 121495. https://doi.org/10.1016/j.lfs.2023.121495

[17] CHEN Z, HALFORD NG, LIU C. Real-Time Quantitative PCR: Primer Design, Reference Gene Selection, Calculations and Statistics. Metabolites 2023; 13: 806. https://doi.org/10.3390/metabo13070806

[18] XIA Y, JIN Y, CUI D, WU X, SONG C et al. Antitumor Effect of Simvastatin in Combination With DNA Methyltransferase Inhibitor on Gastric Cancer via GSDME-Mediated Pyroptosis. Front Pharmacol 2022; 13: 860546. https://doi.org/10.3389/fphar.2022.860546

[19] LONG Y, WANG Z, FAN J, YUAN L, TONG C et al. A hybrid membrane coating nanodrug system against gastric cancer via the VEGFR2/STAT3 signaling pathway. J Mater Chem B 2021; 9: 3838-3855. https://doi.org/10.1039/d1tb00029b

[20] XU X, QIU H. BRD4 promotes gouty arthritis through MDM2-mediated PPARγ degradation and pyroptosis. Mol Med 2024; 30: 67. https://doi.org/10.1186/s10020-024-00831-w

[21] HU T, CAI H, DUAN X, ZHUANG Y. Inhibition of MDM2 by nutlin-3 decreased pyroptosis but increased apoptosis of lung carcinoma cells under 5-FU chemotherapy. J Cancer Res Ther 2025; 21: 1186-1197. https://doi.org/10.4103/jcrt.jcrt_2060_24

[22] CHINNAM M, XU C, LAMA R, ZHANG X, CEDENO CD et al. MDM2 E3 ligase activity is essential for p53 regulation and cell cycle integrity. PLoS Genet 2022; 18: e1010171. https://doi.org/10.1371/journal.pgen.1010171

[23] ZHANG S, XU H, LI W, JI J, JIN Q et al. MDM2 promotes cancer cell survival through regulating the expression of HIF-1α and pVHL in retinoblastoma. Pathol Oncol Res 2023; 29: 1610801. https://doi.org/10.3389/pore.2023.1610801

[24] ZHANG L, ZHU D, JIANG J, MIN Z, FA Z. The ubiquitin E3 ligase MDM2 induces chemoresistance in colorectal cancer by degradation of ING3. Carcinogenesis 2023; 44: 562-575. https://doi.org/10.1093/carcin/bgad040

[25] CATAPANO MS, MARX JA. Central nervous system cysticercosis simulating an acute cerebellar hemorrhage. Ann Emerg Med 1986; 15: 847-849. https://doi.org/10.1016/s0196-0644(86)80389-4
[26] LIU Y, CHEN P, QI D, CHEN L. Glaucocalyxin A Inhibits the Malignancies of Gastric Cancer Cells by Downregulating MDM2 and RNF6 via MiR-3658 and the SMG1-UPF mRNA Decay Pathway. Front Oncol 2022; 12: 871169. https://doi.org/10.3389/fonc.2022.871169
[27] MOHAMMADIAN M, ROSTAMZADEH KHAMENEH Z, EMAMGHOLIZADEH MINAEI S, EBRAHIMIFAR M, ESGANDARI K. Regulatory Effects of Apatinib in Combination with Piperine on MDM-2 Gene Expression, Glutathione Peroxidase Activity and Nitric Oxide level as Mechanisms of Cytotoxicity in Colorectal Cancer Cells. Adv Pharm Bull 2022; 12: 404-409. https://doi.org/10.34172/apb.2022.040
[28] VASUDEVAN SO, BEHL B, RATHINAM VA. Pyroptosis-induced inflammation and tissue damage. Semin Immunol 2023; 69: 101781. https://doi.org/10.1016/j.smim.2023.101781
[29] BROZ P. Pyroptosis: molecular mechanisms and roles in disease. Cell Res 2025; 35: 334-344. https://doi.org/10.1038/s41422-025-01107-6
[30] WU J, WANG L, XU J. The role of pyroptosis in modulating the tumor immune microenvironment. Biomark Res 2022; 10: 45. https://doi.org/10.1186/s40364-022-00391-3
[31] WANG H, WANG T, YAN S, TANG J, ZHANG Y et al. Crosstalk of pyroptosis and cytokine in the tumor microenvironment: from mechanisms to clinical implication. Mol Cancer 2024; 23: 268. https://doi.org/10.1186/s12943-024-02183-9
[32] WANG G, LI Y, GUO Z, HE Q, LIU Z et al. Tanshinone I Stimulates Pyroptosis of Cisplatin-Resistant Gastric Cancer Cells by Activating the NF-κB/Caspase-3(8)/GSDME Signaling Pathway. DNA Cell Biol 2024; 43: 185-196. https://doi.org/10.1089/dna.2023.0293
[33] XIE W, ZHANG L, SHEN J, LAI F, HAN W et al. Knockdown of CENPM activates cGAS-STING pathway to inhibit ovarian cancer by promoting pyroptosis. BMC Cancer 2024; 24: 551. https://doi.org/10.1186/s12885-024-12296-5
[34] LI S, YUE M, XU H, ZHANG X, MAO T et al. Chemotherapeutic drugs-induced pyroptosis mediated by gasdermin E promotes the progression and chemoresistance of pancreatic cancer. Cancer Lett 2023; 564: 216206. https://doi.org/10.1016/j.canlet.2023.216206
[35] WANG J, SU H, WANG M, WARD R, AN S et al. Pyroptosis and the fight against lung cancer. Med Res Rev 2025; 45: 5-28. https://doi.org/10.1002/med.22071
[36] HARONIKOVA L, BONCZEK O, ZATLOUKALOVA P, KOKAS-ZAVADIL F, KUCERIKOVA M et al. Resistance mechanisms to inhibitors of p53-MDM2 interactions in cancer therapy: can we overcome them? Cell Mol Biol Lett 2021; 26: 53. https://doi.org/10.1186/s11658-021-00293-6

Figure Legends

Figure 1. Effects of Apatinib and Cinobufagin (CS-1) on cell viability, proliferation, and migration in gastric cancer (GC) cells. A-D) The effects of different concentrations of Apatinib (1, 2.5, 5, 10 and 20 μM) and CS-1 (0.01, 0.025, 0.05, 0.1 and 0.2 μM) on the viability of GC cells was detected

by Cell counting kit-8 (CCK-8) assays. E-H) Median-effect analysis of the combination of apatinib and CS-1 at a fixed ratio of 100:1. I, J) CCK-8 assays measuring cell viability in AGS and GPM-1 cells treated with control (Con), Apatinib, CS-1, or Apatinib+CS-1. K-M) Colony formation assays assessing cell proliferation in AGS and GPM-1 cells treated with Con, Apatinib, CS-1, or Apatinib+CS-1. Data are presented as mean±standard deviation (n=3 independent biological replicates). *$p < 0.05$, **$p < 0.01$, ***$p < 0.001$ vs. Con; $^{\#\#}p < 0.01$, $^{\#\#\#}p < 0.001$ vs. Apatinib; $^{\&\&}p < 0.01$, $^{\&\&\&}p < 0.001$ vs. CS-1

Figure 2. Apatinib and CS-1 promote apoptosis and reduce stemness in GC cells. A-C) Wound healing assays evaluating cell migration in AGS and GPM-1 cells treated with Con, Apatinib, CS-1, or Apatinib+CS-1. Scale bars, 100 μm; magnification, 100×. D-F) Flow cytometric analysis of apoptosis in AGS and GPM-1 cells treated with Con, Apatinib, CS-1, or Apatinib+CS-1. G-I) Sphere formation assays assessing cellular stemness in AGS and GPM-1 cells treated with Con, Apatinib, CS-1, or Apatinib+CS-1. Scale bars, 100 μm; magnification, 200×. Data are presented as mean±standard deviation (n=3 independent biological replicates). *$p < 0.05$, **$p < 0.01$, ***$p < 0.001$ vs. Con; $^{\#\#}p < 0.01$, $^{\#\#\#}p < 0.001$ vs. Apatinib; $^{\&\&}p < 0.01$, $^{\&\&\&}p < 0.001$ vs. CS-1

Figure 3. Regulation of mouse double minute 2 homolog (MDM2) and pyroptosis-related proteins by Apatinib and CS-1. A, B) Reverse transcription quantitative polymerase chain reaction (RT-qPCR) analysis of MDM2 mRNA levels in AGS and GPM-1 cells treated with Con, Apatinib, CS-1, or Apatinib+CS-1. Glyceraldehyde-3-phosphate dehydrogenase (GAPDH) served as the internal control. C-J) Western blot analysis of MDM2, cleaved caspase-3 (C-caspase-3), and gasdermin E-N (GSDME-N) protein levels in AGS and GPM-1 cells treated with Con, Apatinib, CS-1, or Apatinib+CS-1. GAPDH was used as the loading control. Data are presented as mean±standard deviation (n=3 independent biological replicates). **$p < 0.01$, ***$p < 0.001$ vs. Con; $^{\#}p < 0.05$, $^{\#\#}p < 0.01$, $^{\#\#\#}p < 0.001$ vs. Apatinib; $^{\&}p < 0.05$, $^{\&\&}p < 0.01$, $^{\&\&\&}p < 0.001$ vs. CS-1

Figure 4. MDM2 mediates the effects of Apatinib and CS-1 on cell viability, proliferation, and migration in GC cells. A, B) RT-qPCR validation of MDM2 overexpression in AGS and GPM-1 cells. C, D) CCK-8 assays measuring cell viability in AGS and GPM-1 cells treated with Con,

Apatinib+CS-1, Apatinib+CS-1+negative control (oe-NC), and Apatinib+CS-1+oe-MDM2. E, G-H) Colony formation assays evaluating cell proliferation in AGS and GPM-1 cells treated with Con, Apatinib+CS-1, Apatinib+CS-1+oe-NC, and Apatinib+CS-1+oe-MDM2. (F, I-J) Wound healing assays assessing migration ability in AGS and GPM-1 cells treated with Con, Apatinib+CS-1, Apatinib+CS-1+oe-NC, and Apatinib+CS-1+oe-MDM2. Scale bars, 100 μm; magnification, 100×. Data are presented as mean±standard deviation (n=3 independent biological replicates). $^{+++}p < 0.001$ vs. oe-NC; $^{**}p < 0.01$, $^{***}p < 0.001$ vs. Con; $^{\Delta}p < 0.05$, $^{\Delta\Delta\Delta}p < 0.001$ vs. Apatinib+CS-1+oe-NC

Figure 5. MDM2 modulates apoptosis, stemness, and pyroptosis-related protein expression in GC cells treated with Apatinib and CS-1. A-C) Flow cytometric analysis of apoptosis in AGS and GPM-1 cells treated with Con, Apatinib+CS-1, Apatinib+CS-1+oe-NC, and Apatinib+CS-1+oe-MDM2. D-F) Sphere formation assays to assess stemness in AGS and GPM-1 cells treated with Con, Apatinib+CS-1, Apatinib+CS-1+oe-NC, and Apatinib+CS-1+oe-MDM2. Scale bars, 100 μm; magnification, 200×. G-J) Western blot analysis of GSDME-N and C-caspase-3 expression in AGS and GPM-1 cells treated with Con, Apatinib+CS-1, Apatinib+CS-1+oe-NC, and Apatinib+CS-1+oe-MDM2. GAPDH served as the internal control. Data are presented as mean±standard deviation (n=3 independent biological replicates). $^{*}p < 0.05$, $^{***}p < 0.001$ vs. Con; $^{\Delta}p < 0.05$, $^{\Delta\Delta\Delta}p < 0.001$ vs. Apatinib+CS-1+oe-NC

Figure 6. MDM2 overexpression attenuates the antitumor effects of Apatinib and CS-1 *in vivo*. A) Tumor images of each group of mice. B) Tumor volume measurements in mice from the Con+oe-NC, Apatinib+CS-1+oe-NC, and Apatinib+CS-1+oe-MDM2 groups on days 3, 5, 7, 9, 11, 13, 15, and 17. C) Terminal deoxynucleotidyl transferase dUTP nick-end labeling (TUNEL) assay of tumor sections to detect apoptotic cells in Con+oe-NC, Apatinib+CS-1+oe-NC, and Apatinib+CS-1+oe-MDM2 groups. Scale bars, 50 μm; magnification, 400×. D) Immunohistochemistry analysis of Ki67 expression in tumor tissues of Con+oe-NC, Apatinib+CS-1+oe-NC, and Apatinib+CS-1+oe-MDM2 groups. Scale bars, 100 μm; magnification, 400×. E-G) Western blot analysis of GSDME-N and C-caspase-3 expression in tumor tissues of Con+oe-NC, Apatinib+CS-1+oe-NC, and Apatinib+CS-1+oe-MDM2 groups. GAPDH was used as

the internal control. Data are presented as mean±standard deviation (n=8/group). $^{\theta}p < 0.05$, $^{\theta\theta}p < 0.01$, $^{\theta\theta\theta}p < 0.001$ vs. Con+oe-NC; $^{\Delta}p < 0.05$, $^{\Delta\Delta}p < 0.01$, $^{\Delta\Delta\Delta}p < 0.001$ vs. Apatinib+CS-1+oe-NC

505 **Table 1.** Primers used for real- time PCR in this study.

Genes	Forward primer (5'-3')	Reverse primer (5'-3')
MDM2	CACCTCACAGATTCCAGCTT	CGCCAAACAAATCTCCTAGA
GAPDH	AACGGATTTGGTCGTATTGGG	CGCTCCTGGAAGATGGTGAT

506

507 **Table 2.** Antibodies used in western blot analysis.

Antibody name	Molecular weight	Source	Catalog Number	Supplier	Type	Dilution
MDM2	55, 58 kDa	Rabbit	ab259265	Abcam	Primary antibody	1:1000
GSDME-N	35 kDa	Rabbit	ab222408	Abcam	Primary antibody	1:1000
c-Caspase 3	17 kDa	Rabbit	ab32042	Abcam	Primary antibody	1:1000
GAPDH	34 kDa	Mouse	ab8245	Abcam	Primary antibody	1:5000
Goat Anti-Rabbit IgG H&L (HRP)			ab6721	Abcam	Secondary antibody	1:5000
Goat Anti-Mouse IgG H&L (HRP)			ab205719	Abcam	Secondary antibody	1:5000

508

509 **Table 3.** Combination index (CI) values of apatinib and CS-1 in gastric cancer cells.

Cell line	Apatinib (μM)	CS-1 (μM)	Inhibition rate (%)	CI
GPM-1	5	0.05	62	0.37
GPM-1	10	0.1	74	0.56
GPM-1	20	0.2	81	0.78
AGS	5	0.05	64	0.57
AGS	10	0.1	70	0.62
AGS	20	0.2	77	0.80

510

Fig. 1 Download full resolution image

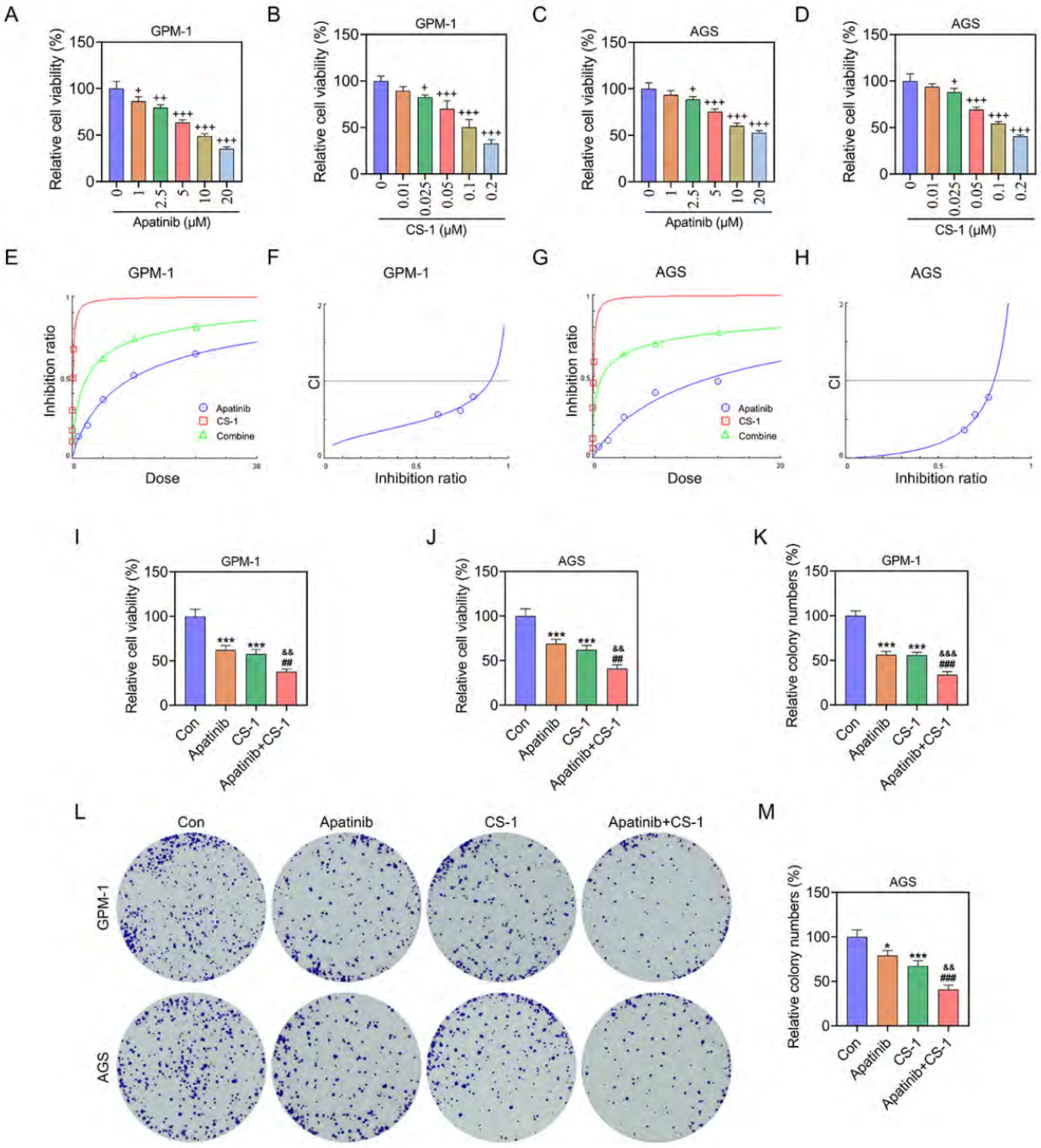

Fig. 2 [Download full resolution image]

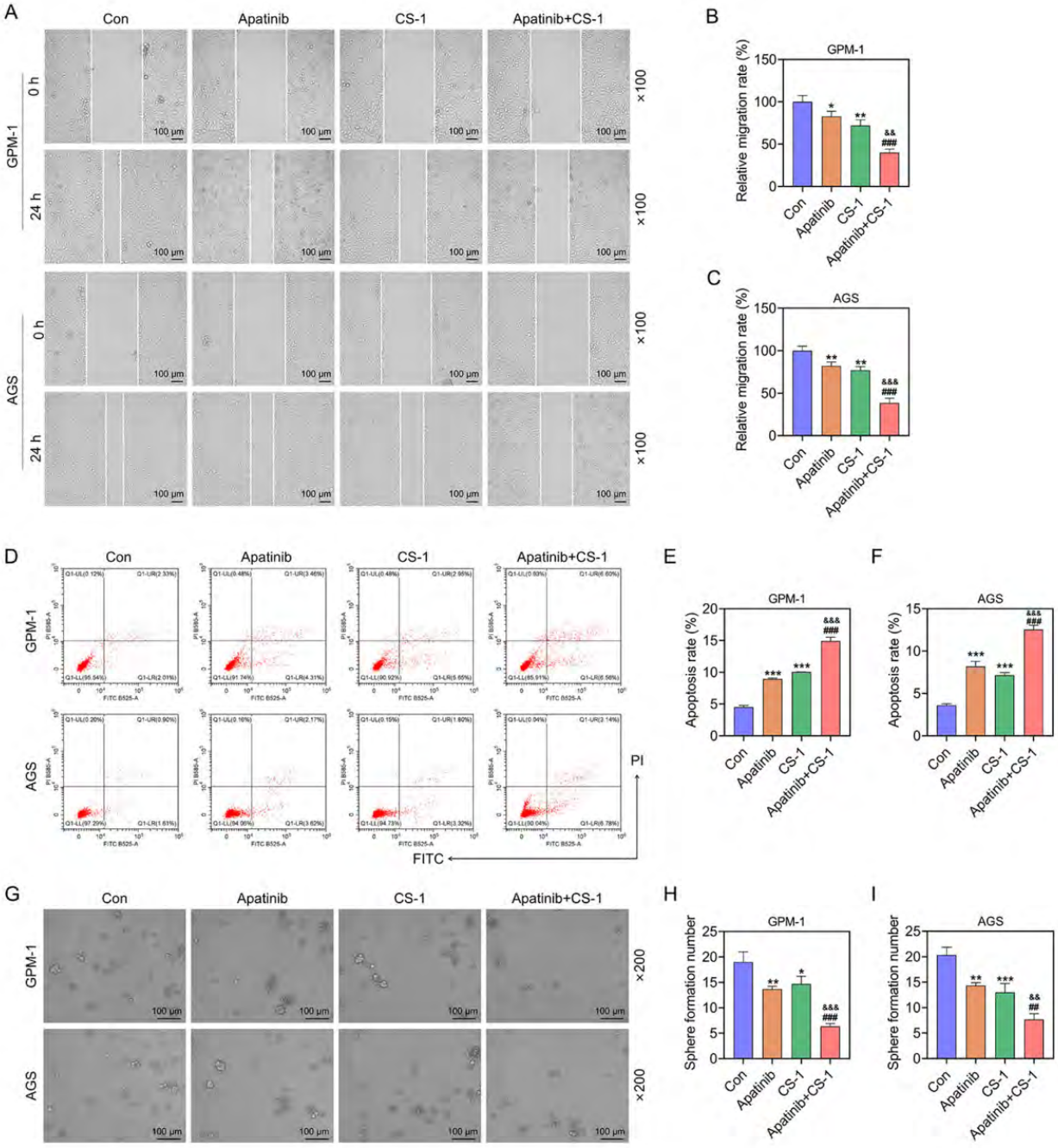

Fig. 3 [Download full resolution image]

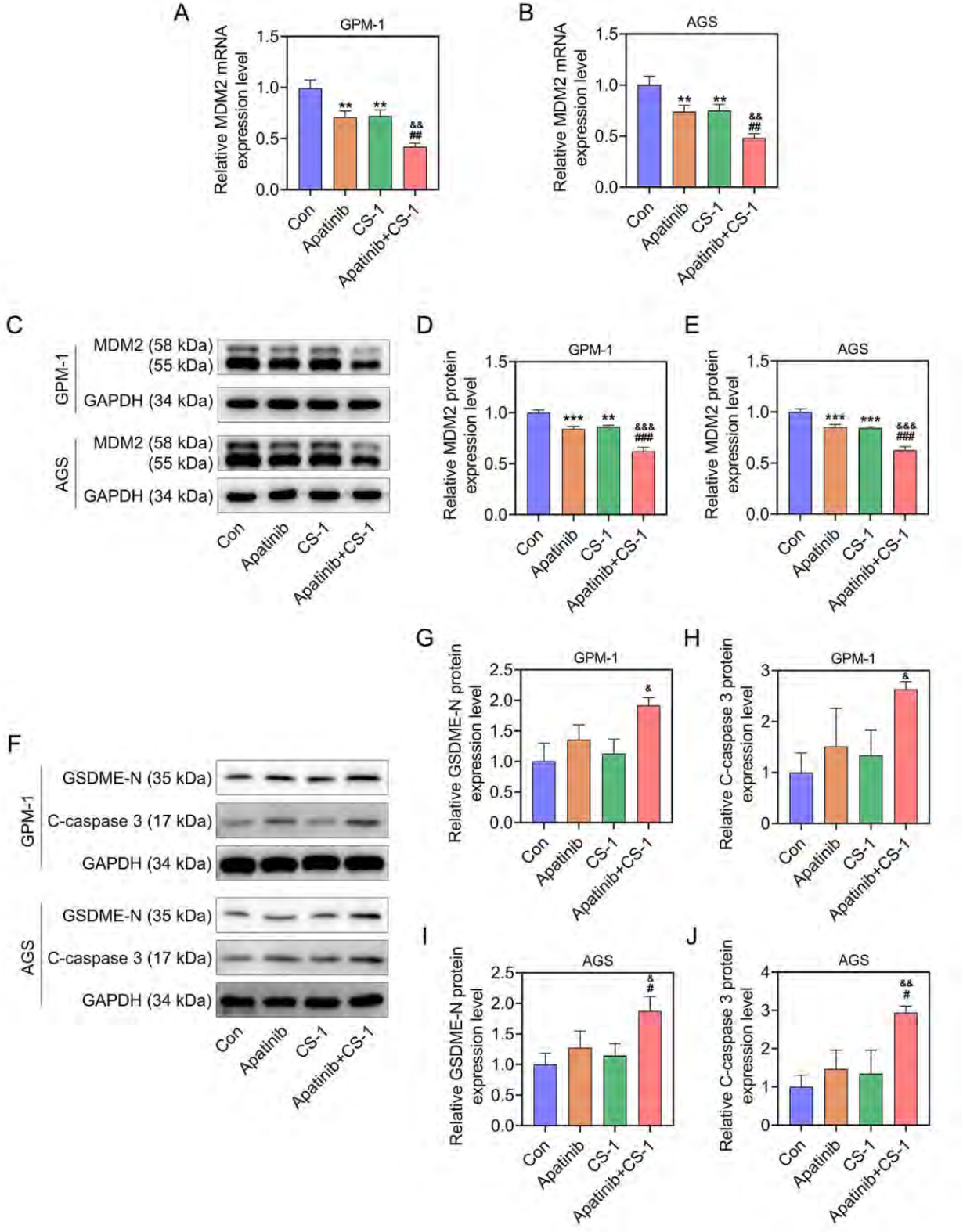

Fig. 4 [Download full resolution image]

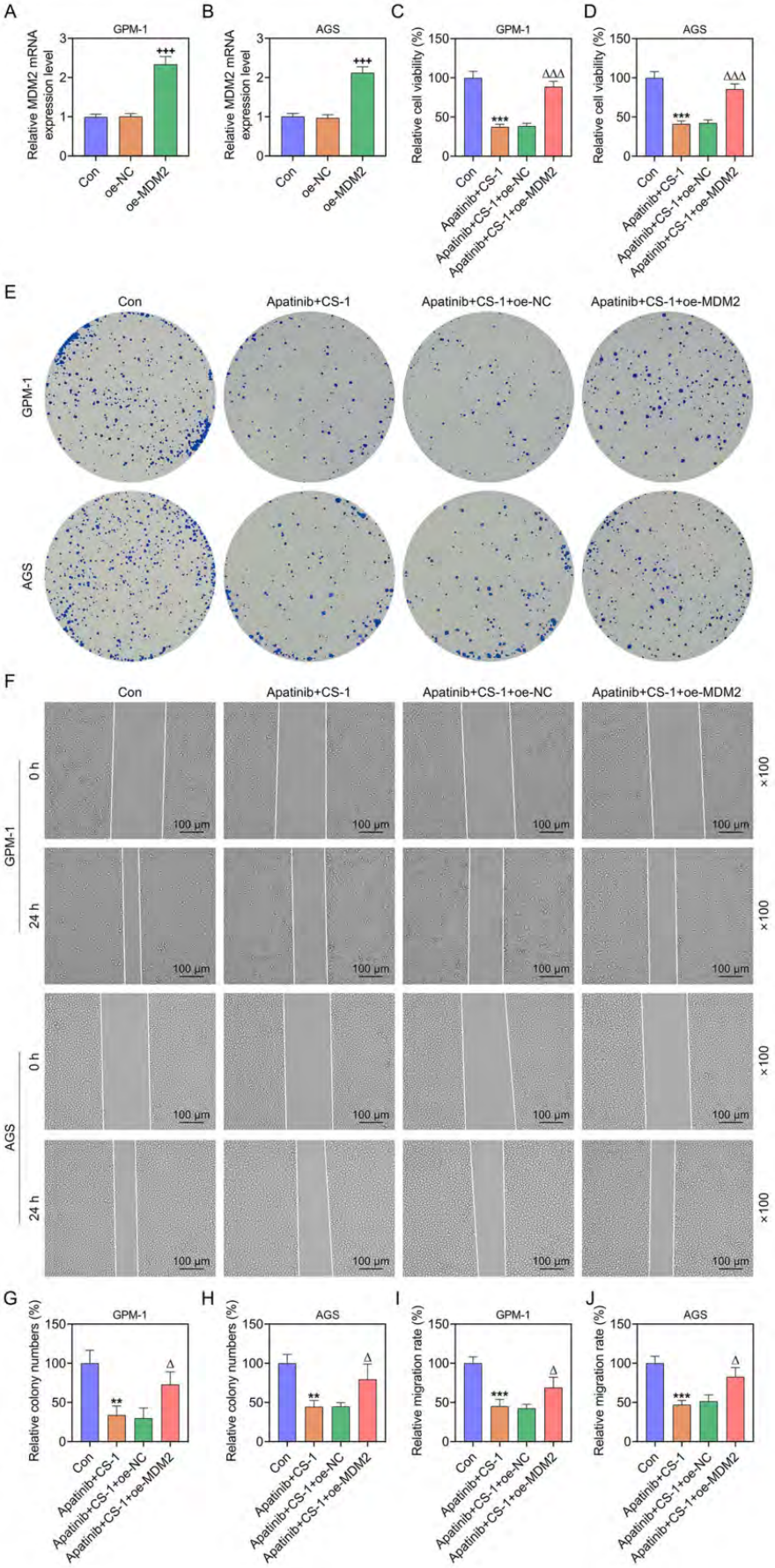

Fig. 5 Download full resolution image

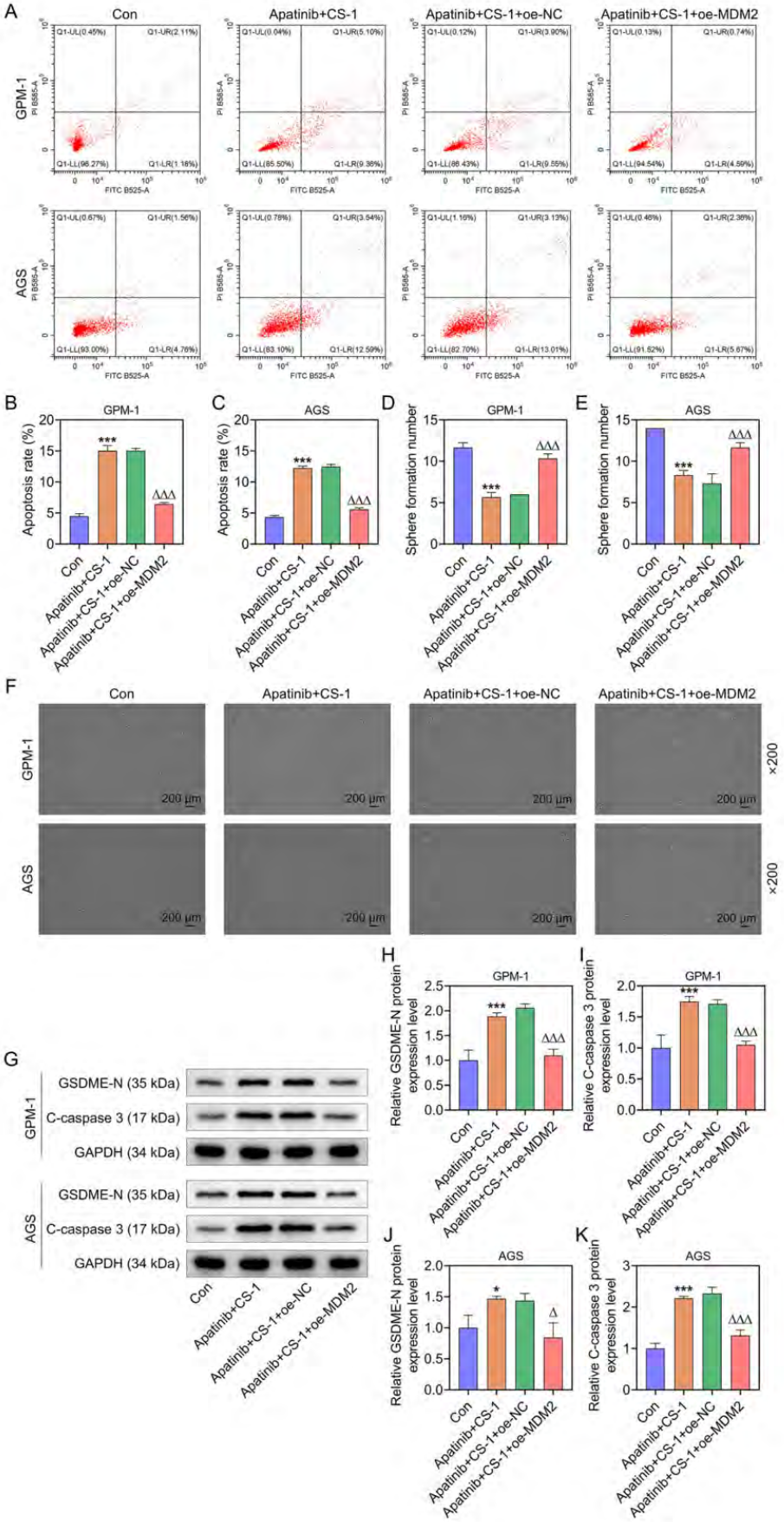

Fig. 6 Download full resolution image